Water Research 155 (2019) 225–232

Contents lists available at ScienceDirect

Water Research

journal homepage: www.elsevier.com/locate/watres

Hazardous waste dewatering and dry mass reduction through hydrophobic modification by a facile one-pot, alkali-assisted hydrothermal reaction

Xiang Li [a, b, **], Jing Wang [a], Jiguang You [a], Pingfeng Yu [b], Xianying Li [a], Gang Xue [a, c, ***], Hong Chen [a], Xianbao Xu [a], Sjack van Agtmaal [d], Pedro J.J. Alvarez [b, *]

[a] State Environmental Protection Engineering Centre for Pollution Treatment and Control in Textile Industry, College of Environmental Science and Engineering, Donghua University, 2999 North Renmin Road, Shanghai, 201620, China
[b] Department of Civil and Environmental Engineering, Rice University, Houston, TX, 77005, United States
[c] Shanghai Institute of Pollution Control and Ecological Security, Shanghai, 200092, China
[d] BCF Systems for Separation Processes Ltd, Olmendreef 2a, Steenbergen, 4651 RP, the Netherlands

ARTICLE INFO

Article history:
Received 2 February 2019
Received in revised form
21 February 2019
Accepted 25 February 2019
Available online 26 February 2019

Keywords:
Hazardous waste
Dewatering
Hydrothermal treatment
Paint sludge
Hydrophobic

ABSTRACT

Hazardous waste dewatering is important for volume reduction and further treatment. Hazardous organic wastes with low ratio of free to bound water, and low flash point are difficult to dewater and pose an explosion risk for conventional thermal drying. Here, we develop a facile one-pot, alkali-assisted hydrothermal treatment (AHT) method for cost-efficient hazardous waste dewatering, dry mass minimization and volume reduction. Wet paint sludge (WPS), a hazardous organic waste, was reduced (79% by total weight and 52% by dry mass) by dewatering through AHT hydrophobic modification, and the product was nonflammable. Conversion of bound water to free water enhanced WPS dissolution for further decomposition. Alkali was critical for boosting ether demethylation in the solid phase, and cleavage of ethers forming alcohols that facilitated transfer of solid mass into the liquid phase. Polar functional groups were eliminated through AHT, which increased the relative abundance of hydrophobic functional groups on the surface of solid residues and promoted dewatering. We also demonstrate that AHT can be widely adapted and scaled up to treat various hazardous organic waste streams, which is of significant industrial and environmental interest.

1. Introduction

Hazardous wastes, which are characterized by their ignitability, corrosivity, reactivity and/or toxicity, are generated in large quantities from industrial manufacturing process (D'Alisa et al., 2014; Daniels, 1986). Disposal of hazardous waste is often outsourced to licensed incineration facilities that are approaching their treatment capacities (Walser et al., 2012) (Garcia-Labiano et al., 2007). Furthermore, hazardous wastes disposal represents a significant, quantity-dependent cost (Table S1). Considering the growing amounts of hazardous wastes being generated, rising disposal costs, and public opposition to the siting of new disposal facilities, it is important to develop strategies for waste volume reduction (e.g., through enhanced dewatering) that also facilitate further treatment in a safe and cost-effective manner (Lim et al., 2011; Xu et al., 2018).

Most chemical process industries (e.g., refineries, pharmaceutical, automotive, and textile) use water, solvents and polymers, that end up in their hazardous wastes (Dmitrienko and Strizhak, 2018; Yin et al., 2015; Zhang et al., 2007; Zhu et al., 2018). These industries generate large quantities of hazardous organic waste (often volatile sludge) with a large fraction of non-drainable moisture; i.e., low ratio of free to bound water (Guo et al., 2019;

* Corresponding author.
** Corresponding author. State Environmental Protection Engineering Centre for Pollution Treatment and Control in Textile Industry, College of Environmental Science and Engineering, Donghua University, 2999 North Renmin Road, Shanghai, 201620, China.
*** Corresponding author. State Environmental Protection Engineering Centre for Pollution Treatment and Control in Textile Industry, College of Environmental Science and Engineering, Donghua University, 2999 North Renmin Road, Shanghai, 201620, China.
E-mail addresses: lix@dhu.edu.cn (X. Li), xuegang@dhu.edu.cn (G. Xue), alvarez@rice.edu (P.J.J. Alvarez).

https://doi.org/10.1016/j.watres.2019.02.050
0043-1354/

Xiao et al., 2018). Bound water, which significantly contributes to waste volume, is held tightly to the polar groups or ionic sites on molecules, and cannot be squeezed out by conventional dewatering technologies such as high-pressure plate and frame filter pressing, belt press filtering and centrifuge processing (Christensen et al., 2015). Thermal drying processes (TDP) are often used to evaporate moisture from the dewatered wastes (Bennamoun et al., 2013). However, separating water from the hazardous organic waste by TDP suffers from low energy efficiency (Zhang et al., 2014), and poses an explosion hazard due to the low flash point of these wastes (Liaw et al., 2010; Salihoglu and Salihoglu, 2016). Note that dewatering is important to reduce the waste volume through solid-liquid separation, but it does not per se achieve dry mass reduction (Christensen et al., 2015). This underscores the need for broadly applicable and cost-effective treatment approaches that reduce both the volume and dry mass of hazardous organic sludges.

Hydrothermal treatment (HT), which is conducted in a closed reactor at 180–350 °C under autogenous pressure, offers a reliable route to convert waste activated sludge into value-added products (Higgins et al., 2017; Li et al., 2017) and facilitate dewatering due to decomposition of water-binding components (Yu et al., 2014) and dehydration reactions (Wang and Li, 2015). However, the feasibility of HT for hazardous sludge volume reduction and dry mass removal has not been addressed in the literature. Since depolymerization, decomposition and solubilization of organic wastes (e.g., using supercritical fluids) contribute to dry mass reduction (Chen et al., 1995; Demirbas, 2010; Staszak and Malinowski, 1987), it is essential to promote these reactions in the mild hydrothermal process. The benefits of HT treatment on depolymerization has been documented only in the presence of large amounts of olefin metathesis over long reaction periods (i.e., 4 d) (Jia et al., 2016) or intensive energy input to achieve high temperatures (>400 °C) (Aguado et al., 2008; Serrano et al., 2012) with microwave-assistance (Fan et al., 2013). However, alkaline conditions decrease the polarity of organic matter and facilitate the hydrolytic cleavage of carbon-functional groups under milder conditions (Comisar et al., 2008; Mursito et al., 2011; Roberts et al., 2010). Thus, we envisioned that alkali addition might assist HT treatment to enhance dry mass reduction.

Since paint is broadly applied in industry, wet paint sludge (WPS) is a common hazardous organic waste that is generated in large and increasing quantities (Salihoglu and Salihoglu, 2016; Akafuah et al., 2013). This paper reports WPS volume and dry mass reduction through a facile one-pot alkaline hydrothermal (AHT) method. A systematic investigation was conducted to discern the underlying mechanisms for hydrophobic modification of WPS to convert bound water to easily drainable free water. The reaction pathway was investigated to discern the critical role of alkali for dry mass reduction. Furthermore, pilot-scale tests were operated with a variety of other hazardous wastes to demonstrate AHT as a reliable, industrially-scalable and broadly applicable process.

2. Materials and methods

2.1. Wet paint sludge (WPS) and other hazardous wastes

WPS was obtained from an automotive lock company (Shanghai, China). It has a sticky, paste-like consistency with a significant non-drainable moisture content (77.5%) and a high volatile solid to total solid ratio (VS/TS 83.5%), reflected by its relatively low ratio of free to bound water ($W_f = 1.10$ g/g dry mass, Fig. S1 by Differential Scanning Calorimetry (DSC)) and flash point (67.1 °C, Table S2). To evaluate the alkali-assisted hydrothermal treatment as a broadly applicable technique, the following hazardous wastes were chosen: oil sludge, pharmaceutical residues, high boiling residues from distillation towers, concentrated solutions from the fluorine industry, and textile sludge (Fig. S2). These hazardous organic wastes are characterized by high moisture content (57.8–85.4%) and high VS/TS ratio (64.3–93.4%) as detailed in Table S3. Waste samples were stored at 4 °C prior to use.

2.2. Selection of hydrothermal reaction parameters using response surface methodology

A preliminary study (see Supplementary Information) verified that temperature and reaction time are crucial parameters in hydrothermal treatment (HT) for WPS dewatering (Fig. S3). Using Design Expert Software (version 8.05, Stat-Ease, Inc., USA), a five-level, two-variable central composite design (CCD, Table 1) was adopted to select the HT parameters. Hydrothermal batch reactions were conducted by loading 25 g of WPS in 100-mL airtight stainless-steel tubular reactor (polyphenylene container inside) (Fig. S4a). The reactors were heated to the selected temperatures (variable A, Table 1) in a homothermic oven (DHG-9013A). After a stipulated time period (variable B, Table 1), these reactors were cooled to room temperature in water bath. The samples were withdrawn from the containers, and dewatered by vacuum filtration (Fig. S4a) for 3 min. Then, the residues on the filter paper were weighed. The residues were dried in a homothermic oven (DHG-9013A) at 105 °C for 24 h for dry mass measurement. All tests were performed in triplicate, and the results were expressed as mean ± standard deviation. The total mass reduction (TMR) of WPS was calculated using Eq (1), whereas dry mass reduction (DMR) using Eq (2).

$$TMR = [(m_1\text{-}m_2)/m_1]^*100\% \quad (1)$$

$$DMR = [(m_3\text{-}m_4)/m_3]^*100\% \quad (2)$$

Where m_1 is the weight of raw waste; m_2 is the weight of solid residues in the filter paper after vacuum filtration; m_3 is the dry weight of raw WPS; and m_4 is the dry weight of the solid residues after vacuum filtration.

Regression analysis yielded predictive polynomial quadratic models (Table S4) for both responses (TMR and DMR). Response surface methodology showed that the interacting effects of temperature and time on total mass reduction (TMR) ($p < 0.09$) and dry mass reduction (DMR) ($p < 0.08$) were significant (Table S5, Fig. S5). TMR increased rapidly from 50% to 71% by increasing the temperature from 180 to 220 °C and time from 3 to 4 h (Fig. 1a), and it increased slowly to 75% with longer duration (>4 h) at a higher temperature (>220 °C). However, DMR only increased with

Table 1
Experiments designed by CCD and the responses of TMR and DMR.

Run	Variable A Temperature (°C)	Variable B Time (h)	TMR(%)	DMR(%)
1	200	5	69.5	26.7
2	220	4	73.1	38.4
3	260	4	76.1	44.3
4	240	3	70.3	33.4
5	200	3	54.7	24.8
6	220	4	71.2	38.4
7	240	5	75.6	42.3
8	220	4	71.3	36.6
9	220	4	72.8	38.2
10	220	6	72.8	37.5
11	180	4	58.6	16.3
12	220	2	63.3	23.4
13	220	4	72.5	36.3

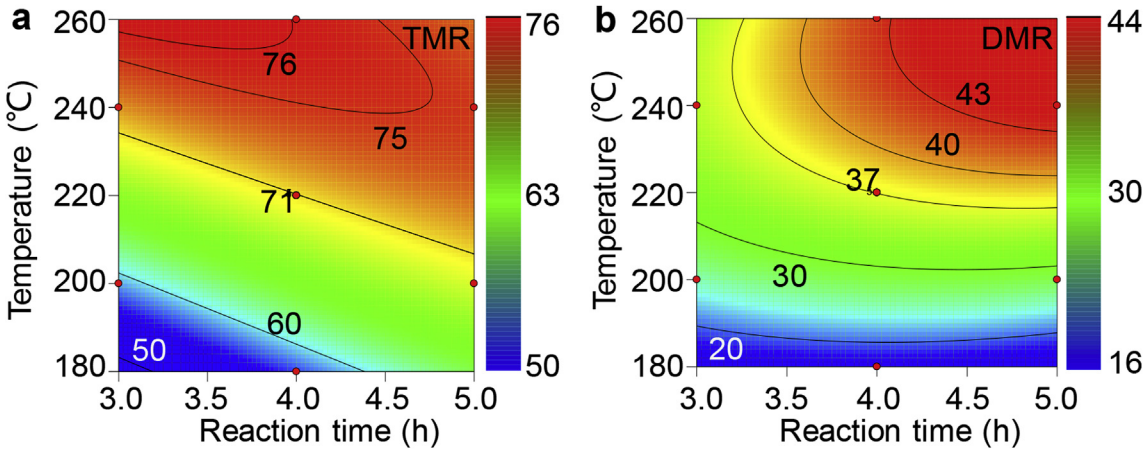

Fig. 1. Response surface methodology for (a) total mass reduction (TMR) and (b) dry mass reduction (DMR) at different temperatures and reaction times.

temperature when the temperature was below 220 °C (Fig. 1b), and it stabilized from 220 to 260 °C at longer reaction times (>4 h). Higher temperature and longer reaction time increase operating and capital costs. Thus, the condition for HT treatment of WPS was selected at 220 °C for 4 h under an autogenous pressure of 385 ± 12 psi.

2.3. Alkali-assisted hydrothermal treatment (AHT) and products characterization

Before hydrothermal treatment, different chemical agents (dosage 50 mg/g WPS) were mixed with 25 g WPS. Unless otherwise noted, the hydrothermal reaction was conducted at a temperature of 220 °C for 4 h. The overall process was the same as described in Section 2.2. Based on this preliminary study (Supplementary Information), dry mass reduction (DMR) of WPS was higher in the reactor with NaOH added than those with other chemical agents (Fig. S6a). The optimal dosage was 38 mg NaOH/g WPS (Fig. S6b) and was selected as the alkali-assisted hydrothermal treatment (AHT) for this study. To advance fundamental understanding of WPS transformations during HT and AHT process, products from both processes were characterized. The liquid collected after filtration was analyzed by GC-MS (Agilent Technologies 7890, USA), gel filtration chromatography (GFC) (Shimadzu Co., Japan), inductively coupled plasma atomic emission spectrometry (ICP-AES) (Prodigy-ICP, USA), and Fourier transform infrared spectroscopy (FTIR) (Nicolet, USA). The residues on the filter paper were characterized by contact angle measurement (Kino, USA), thermogravimetric analysis (TGA) (Mettler, Switzerland), scanning electron microscope (SEM) (JSM-5600LV, Japan), differential scanning calorimetry (DSC) (Mettler, Switzerland), X-ray diffraction (XRD) (Dmax-2550 PC, Japan), zeta potential (Brookhaven ZetaPlus), FTIR, specific surface area by Brunauer-Emmett-Teller (BET) measurement (Quantachrome Autosorb-IQ) and nuclear magnetic resonance (^{13}C solid-state NMR) (AVANCE400, Switzerland).

2.4. Plotting Van Krevelen diagram to propose possible reactions

A Van Krevelen diagram (O/C vs H/C ratios) was used to investigate possible reactions through elemental variations of the molecular composition of solid samples after treatment with different intensities (reaction temperatures, durations and NaOH dosages). Five HT reactors containing raw WPS (25 g) were conducted at different temperatures (140 °C, 180 °C, 200 °C, 220 °C and 240 °C) for 4 h, and another four HT reactors containing raw WPS (25 g) were kept at 220 °C for different durations (2, 3, 4 and 5 h). For AHT reaction, three reactors with different NaOH dosages (0.038, 0.054 and 0.097 g/g WPS) were tested at 220 °C for 4 h. After vacuum filtration, the solid samples were frozen at −20 °C for 24 h, and then sublimated in a freeze-drying machine (Huayu, China) under vacuum for another 24 h. After the freeze-dry process, the powder samples were immediately analyzed using an Elemental Analyzer Vatio EL III (Elementar, German).

2.5. Verification of cleavage of ether bond and depolymerization

Ethylene glycol butyl ether (DEG) and poly(methyl methacrylate) (PMMA) were chosen for evaluation of bond cleavage and depolymerization due to their high abundance in WPS (Table S6 and Table S7). The HT and AHT reactor both contained 2 mL DEG (or 2.5 g PMMA) and 20 mL deionized water and the AHT reactor contained an additional 0.1 g NaOH. After hydrothermal treatment (at 220C for 4 h), the liquids were assayed by GC-MS (Agilent Technologies 7890, USA).

2.6. Effectiveness of AHT on other hazardous wastes and scalability assessment

Hazardous organic wastes mentioned in section 2.1 were treated by AHT: hazardous waste (25 g) and NaOH (0.95 g) were mixed into 100 mL reactors. The reactors were operated at 220 °C for 4 h and the mass reduction was recorded. Five commonly used metal: stainless steel (316 L), Titanium (TA1), Nickel alloys (N6), Zirconium alloy (Zr), and Hastelloy (HC-276) were tested for corrosion resistance to AHT/HT process (Supplementary Information). Each metal coupon was mixed with 25 g WPS in HT reactor (220 °C and 4 h) and AHT reactor (220 °C, 4 h and 38 mg NaOH/g WPS). Corrosion extent was estimated as weight change percentage of the metal coupons after five cycles of the hydrothermal reaction.

The pilot scale system (Fig. S4b) consists of a 50 L jacketed high-pressure stainless steel reactor (GSH-50 L, Zhaoyang Co. LTD, Weihai China), a 50 L flash and cooling tank, and filter press equipment (XAYZ-S/80, Kungong Env. Kunshan China). The pilot scale system was operated by adding 15 ± 2 kg WPS to the jacketed high-pressure reactor (stirring at 50 ± 2 rpm). After hydrothermal treatment for 4 h at 220 °C, the pressure was decreased by conducting flash steam to the flash and cooling tank. After cooling to room temperature, the mixture was pressed by the filter press equipment. The residues obtained in the filter press was weighed.

The dewatering liquor was collected for wastewater treatment (Supplementary Information). Note that AHT process requires the addition of 3.56 L NaOH stock solution (4M), which was replaced by 3.56 L tap water in HT process.

2.7. Analytical methods

The contact angle (θ) was measurement with a goniometer (KINO, USA). A camera integrated with the goniometer was used to record the deionized water droplet added to the sample surface. Free water to bound water ratio was determined through a differential scanning calorimetry (DSC) analyzer (Lee and Lee, 1995) that integrated with a liquid nitrogen cooling system (METTLER, Switzerland). The sample (20 mg) was placed into a special aluminum crucible (40μL) and covered with a lid for each test. Initially, the temperature was cooled to −20 °C. Then, it was increased to 10 °C with a ramp rate of 2 °C/min. The amount of free water was determined by the area of the endothermic curve below the baseline representing the amount of heat required to melt the frozen water. The relationship between the mass of free water and the DSC curve area can be expressed as: $W_f = K^* A$, A is the curves area (mJ/g^{-1}), K is the conversion factor (mg/mJ), determined by obtaining the thermograms of pure water of known mass and measuring the curve area. NMR was used as a qualitative tool to provide information about specific molecular structures and chemical groups. In this work, the ^{13}C NMR (AVANCE400, Switzerland) was used to investigate the solid-state cross-polarization and magic angle spinning nuclear magnetic resonance experiment at a^{13}C frequency: MAS frequency of 8 kHz, contact time of 3 ms. Other analytic methods, including TGA, SEM, Zeta potential, GFC, ICP-AES, FTIR, GC-MS, XRD and BET are detailed in the Supplementary Information.

3. Results and discussion

3.1. Alkali-assisted hydrothermal treatment enhances WPS dewatering and dry mass minimization

Hydrothermal treatment was effective in dewatering WPS, and DMR significantly increased with alkali addition at 38 mg-NaOH/g-WPS (Fig. 2a) from 36.3 ± 1.6% for HT (without NaOH) to 52.1 ± 1.3% for AHT ($p < 0.0005$, Table S8). TMR also significantly increased from 71.5 ± 2.1% for HT to 79.1 ± 3.6% for AHT ($p < 0.05$, Table S9). Removal of organic matter from the solid phase after HT or AHT treatment was corroborated by Difference Thermo-Gravimetry (DTG) from 200 to 350 °C (Fig. 2b and Fig. S7). Based on mass balances, most of the organic matter lost from the solid phase was transferred to the liquid phase. Volatilization of organics (predominantly 1-butanol and camphene, Table S10) was relatively minor (1.4–2.9%, Fig. S8). The beneficial effect of hydrothermal processing on polyethylene (PE) depolymerization has been reported (Jia et al., 2016), although this required large amounts of Re_2O_7/Al_2O_3 catalyst over long reaction periods (i.e., 4 days). Olefin metathesis of the internal double bonds at high temperatures (>400 °C) reduces the PE chain length, forming light alkenes (C3–C5) (Aguado et al., 2008; Serrano et al., 2012). Similarly, cellulose can be depolymerized by hydrothermal processing, with cleavage of the polysaccharide chain and release of CH_2OH proceeding at elevated temperatures (240-260 °C) with microwave-assistance (Fan et al., 2013). Here, we used NaOH to make HT treatment a milder, more eco-friendly and facile process.

3.2. Reaction mechanisms

3.2.1. Hydrophobic modification of solids surface enhanced dewatering and mass reduction

The treated WPS solid was nonflammable (Table S2) and hydrophobic, as evidenced by an increase in the water contact angle (θ) from 13° for Raw WPS (Fig. 3a) to 25° after HT treatment (Fig. 3b) or 107° after AHT treatment (Fig. 3c). The observed decrease in the polarity of the surface reflects a decrease in surface free energy associated with the formation of hydrophobic functional groups, which is consistent with their neutral, non-polar or slightly polar nature (Valsaraj, 1994). Hydrophobic modification of the WPS surface through the AHT process enhanced separation of water from the solids surface much easier, which significantly increased dewaterability compared to raw WPS and HT-treated waste.

The microstructures of the solid samples from WPS before and after treatment by HT or AHT were characterized by scanning electron microscopy (SEM, Fig. S9). The raw WPS had a condensed flaky petrous morphology (Fig. 3d) that changed to a loose packing porous structure with spherical particles (Fig. 3e) after HT treatment. In contrast, residual solid WPS after AHT treatment had an urchin-like structure spread over the surface (Fig. 3f). WPS contains both Si and Zn (Fig. S10), which likely contributed to this morphology; silicate oligomers have been reported to form urchin-like agglomerates under alkaline conditions (Cai et al., 2001), and basicity was reported to play an important role in self-assembly and crystal growth of urchin-like ZnO structures (Jiang et al., 2009). We also observed a crystalline structure after AHT using X-ray diffraction (XRD) analysis (Fig. S11), which was ascribed to alkali serving as a surface modifier for crystal growth (Sahraneshin et al., 2012). The

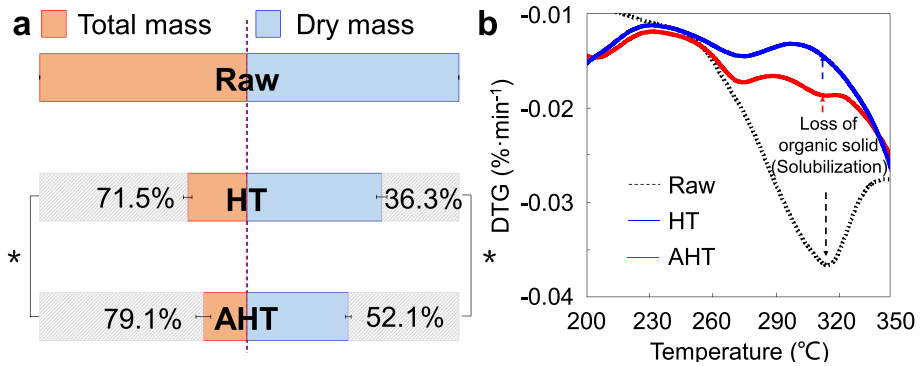

Fig. 2. WPS reduction after HT or AHT treatment. (a) Grey areas represent mass loss compared to the raw WPS, and statistical significance ($p < 0.05$) of TMR and DMR is indicated by asterisks (*); (b) Difference Thermo Gravimetry (DTG) of the solid samples from Raw (dotted), HT (red) and AHT (blue). (For interpretation of the references to colour in this figure legend, the reader is referred to the Web version of this article.)

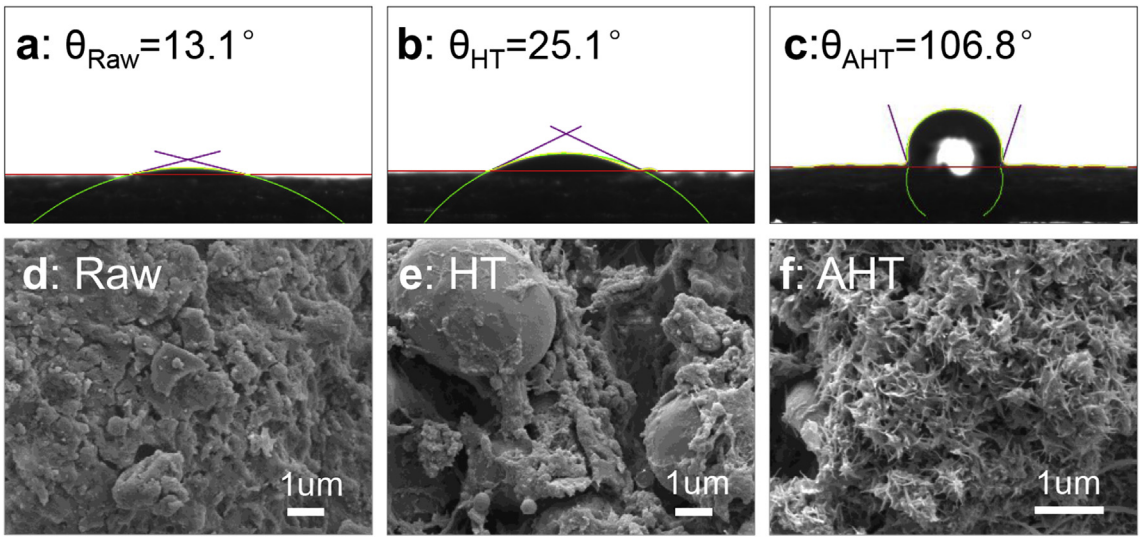

Fig. 3. Surface properties of raw WPS and solid samples after HT and AHT treatment: contact angle (θ) of raw WPS (a), HT product (b), AHT product (c) and SEM images (detailed in Fig. S9) of raw WPS (d), HT solid product (e), and AHT solid product (f).

crystalline structure associated with the urchin-like microstructures affected the surface tension at the interfaces of liquid and solid phases (Sadovnikov and Gusev, 2017), resulting in lower surface energy and hydrophobic surfaces in AHT-treated WPS.

3.2.2. Conversion of bound to free water increased drainable water volume

The temperature increase breaks hydrogen bonds (25–40 kJ/mol) to enable water and alkali to act as solvent and reactant (Akiya and Savage, 2002; Unterlass, 2018). After HT or AHT treatment, the ratio of free to bound water (Wf) increased from 1.10 g/g dry mass for raw WPS to 2.98 g/g dry mass for the HT process product and 4.57 g/g dry mass for the AHT process product (Fig. 4a), which increased the free (drainable) water volume (Fig. S12). AHT (with the increase in temperature) drastically increased the ionic product of water (i.e., K_w) to act as solvent and boost further chemical reactions (Unterlass, 2018). Furthermore, the decrease of the negative charge on the treated solids surface (Table S11) decreased electrostatic repulsion between the particles (Wang and Hu, 2013), thus facilitating particles aggregation and conversion of bound water to free water (Thomas et al., 2017).

3.2.3. Solubilization enhanced dry mass reduction

The chemical oxygen demand (COD) and ammonia concentrations in the aqueous phase were significantly increased by 81- and 70-fold, respectively, after HT treatment and by 112 and 120-fold after AHT treatment (Fig. 4b). This represents deamination and a significant conversion of the organic matter into the aqueous phase ($p < 0.001$, Table S12 and Table S13). Enhanced solubilization of volatile organics was verified by GC-MS (Fig. 4c), showing that the peak intensities of 2-ethyl-1-hexanol and 1-butanol in the liquid after AHT processing were 1.5-fold higher than those in the HT-treated sample. An increase in WPS specific surface area during AHT treatment (Table S14) likely contributed to enhanced solubilization. Depolymerization likely occurred during AHT processing as indicated by the right shift of peaks A-D towards a lower molecular weight (MW) distribution (Fig. 4d). The fraction of smaller MW in the liquid (<1K) dramatically increased after HT (8.2%) and AHT treatment (17.3%) compared to the untreated WPS leachate (0.04%) (Fig. S13). This is consistent with the observation that the released organics in the aqueous phase were biodegradable (Fig. S14), indicating that the generated wastewater was amenable to biological treatment (Supplementary Information). The inorganic metallic components of WPS that are important pigment and driers in paint were also released to the aqueous phase through the HT and AHT treatment processes, and their solubilization was also enhanced under alkaline conditions (Fig. S10).

3.2.4. Proposed reactions for the alkali-assisted hydrothermal process

Examination of the solid phase at the molecular level was also conducted to advance mechanistic understanding of WPS

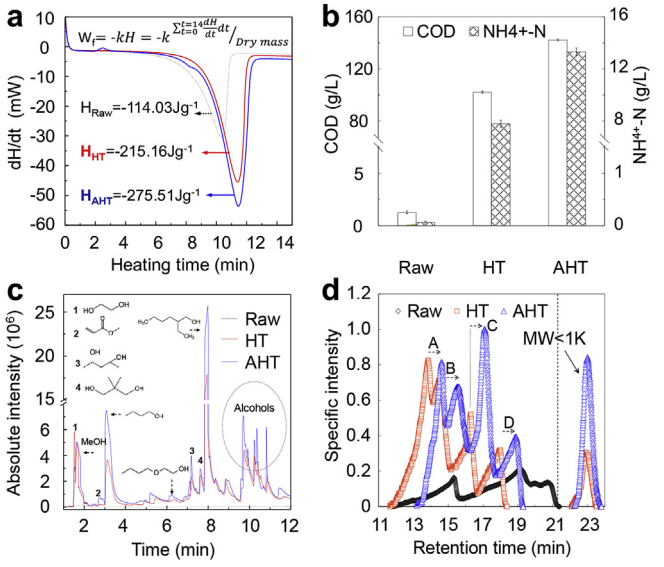

Fig. 4. Dewatering liquor after HT or AHT treatment. (a) DSC thermal profile for raw WPS (grey), HT (red) and AHT product (blue); (b) COD and ammonia-N concentrations in the Raw leachate, after HT or AHT treatment; (c) GC-MS analysis of liquid samples from the raw leachate (grey), after HT (red) or AHT (blue) treatment; (d) MW distribution in the liquid samples from the leachate of raw WPS (grey), after HT (red) or AHT (blue) treatment. Right shift of peaks A-D indicates that AHT sample has smaller MW than HT sample due to greater decomposition associated with AHT treatment. (For interpretation of the references to colour in this figure legend, the reader is referred to the Web version of this article.)

transformations during the AHT process. We propose a series of reactions involving alkaline hydrolysis, dehydration, decarboxylation, depolymerization and demethylation (Fig. 5a) based on the following results. A Van Krevelen diagram (Fig. 5b) reveals that WPS was significantly dehydrated during the HT process following the increase of temperature from 140 to 240 °C (green arrows), which caused a significant loss of oxygen and hydrogen from the WPS solids. WPS decarboxylation, (i.e., disappearance of the COO band, pointed by red arrows), was also observed (red arrows). Furthermore, demethylation (likely due to alkaline hydrolysis of ether bonds) increased with increasing NaOH dosage (blue arrows). DEG, which is an ether used as solvent for paints and varnishes and was abundant in WPS (Table S6), was likely demethylated and degraded to ethylene glycol, n-butanol, 2-butoxyethanol, and 2-ethyl-1-hexanol (Fig. 6). These alcohols accumulated after AHT at 5-fold higher concentrations than after using HT process without alkali (Fig. 5c). Furthermore, methyl methacrylate, the monomer of PMMA which is abundant in WPS (Table S7), appeared in the liquid phase after HT (Fig. 5d), indicating depolymerization (Fig. 6). Methanol was generated when PMMA was treated by AHT (Fig. 5d), since methyl-esterified residues undergo saponification. Overall, alkali boosted ether demethylation in the solid phase, forming alcohols that facilitated transfer of solid mass into the liquid phase.

3.2.5. *Hydrophobic functional groups increased in the solid phase*

FTIR patterns (Fig. 7a) depict changes in the abundance of functional groups among raw WPS, HT and AHT solid products. After HT or AHT treatment, new peaks corresponding to hydrophobic functional groups (pointed by red triangles) became apparent compared to raw WPS. The peaks from the samples after HT or AHT treatment became apparent in the 800-700 cm^{-1} region (CH_2 and CH bending vibrations) and 2970 -2910 cm^{-1} region (aliphatic CH_2 and CH_3 stretching vibrations) compared to raw WPS, which imply a significant hydrophobic character. This observation is consistent with previous reports that an increase in alkali/C ratio shifted the hydrothermal reaction equilibrium of biomass towards hydrophobic products (Allcock, 2008). Furthermore, polar functional groups such as ethers (1150 cm^{-1}), alcohols (3400 cm^{-1}) and amines (3350 cm^{-1}) disappeared from the solid surface after hydrothermal treatment in the presence of NaOH. Basic conditions decreased the polarity of solid surfaces and polarized ether bonds making it easier to cleave heterolytically (Comisar et al., 2008; Mursito et al., 2011; Roberts et al., 2010). Therefore, alkali addition enhanced the transfer of organic matter containing carboxyl, alcohol and ammonia groups from solid to the aqueous phase (Fig. S15). This explains the observed dry mass loss in the volatile organic fraction after AHT processing and the overall conversion to a nonflammable solid residue.

Solid samples from raw WPS, HT and AHT products were characterized by solid-state 13C NMR (Fig. 7b) and showed two similar trends. First, hydrophilic functional groups appeared at chemical shifts (δ) between 113 to 44 and 200 to 161 ppm. Second, hydrophobic functional groups were observed at chemical shifts between 44 to 0 and 161 to 113 ppm (Liu et al., 2015). Because these trends, the HI/HB empirical index of solid hydrophilicity showed a decline from 0.35 (Raw) to 0.34 (HT) and to 0.28 (AHT) (Table 2). The aggregation of hydrophobic groups is conducive to decreasing the number of organized water molecules surrounding them, and this increase in entropy promotes dewatering. This corroborates the vital role of alkali in increasing the number of hydrophobic functional groups on the solids surface, thus promoting further dewatering and solid mass reduction.

3.3. *AHT application to other hazardous organic wastes and pilot scale study*

AHT has broad applicability to treat hazardous organic waste streams from dissimilar industries and resulted in significant TMR and DMR for various hazardous organic wastes (Table S3), including paint sludges from another manufacturer (67.3 ± 1.3% for TMR and 44.5 ± 1.8% for DMR), oil sludge (62.9 ± 2.7% and 21.4 ± 4.8%), pharmaceutical residues (65.1 ± 1.9% and 54.3 ± 2.8%), textile

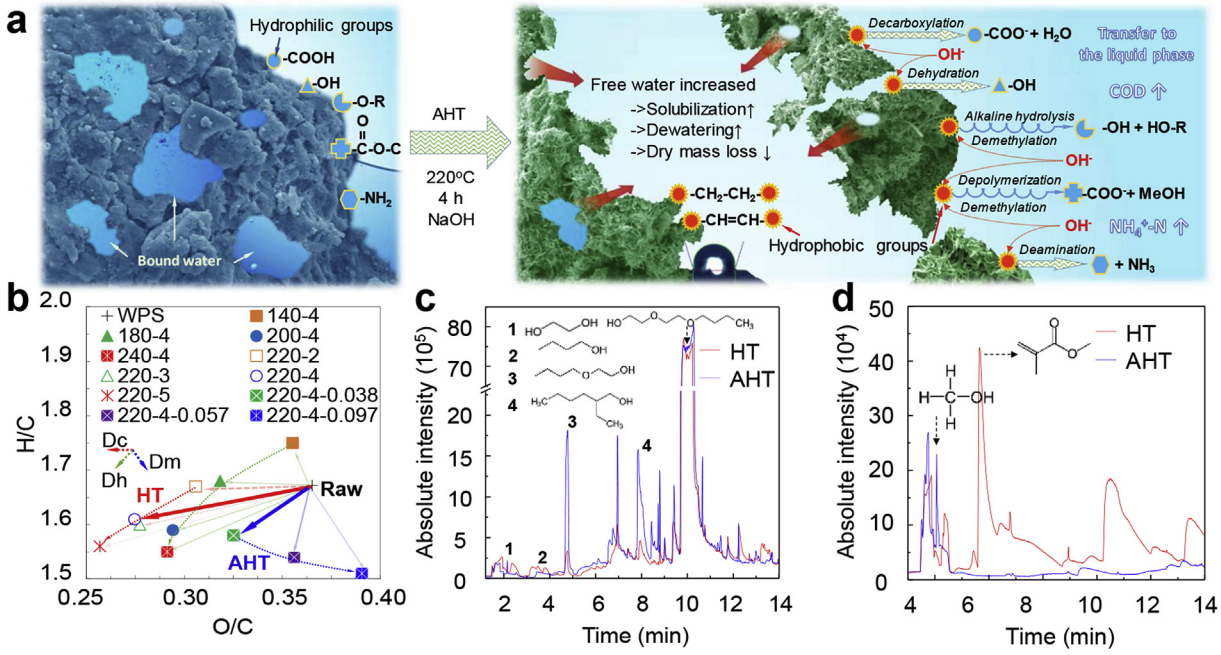

Fig. 5. WPS dewatering and dry mass reduction in HT or AHT process. (a) Proposed reaction mechanisms; (b) Van Krevelen diagram of the solid samples (e.g. 220-4-0.038 represents treatment at 220 °C for 4 h with 38 mg NaOH/g WPS). Dc, Dh, Dm refer to decarboxylation, dehydration and demethylation; and GC-MS analysis of the liquid samples of DEG (c) and PMMA (d) treated by HT(red) or AHT(blue) process. (For interpretation of the references to colour in this figure legend, the reader is referred to the Web version of this article.)

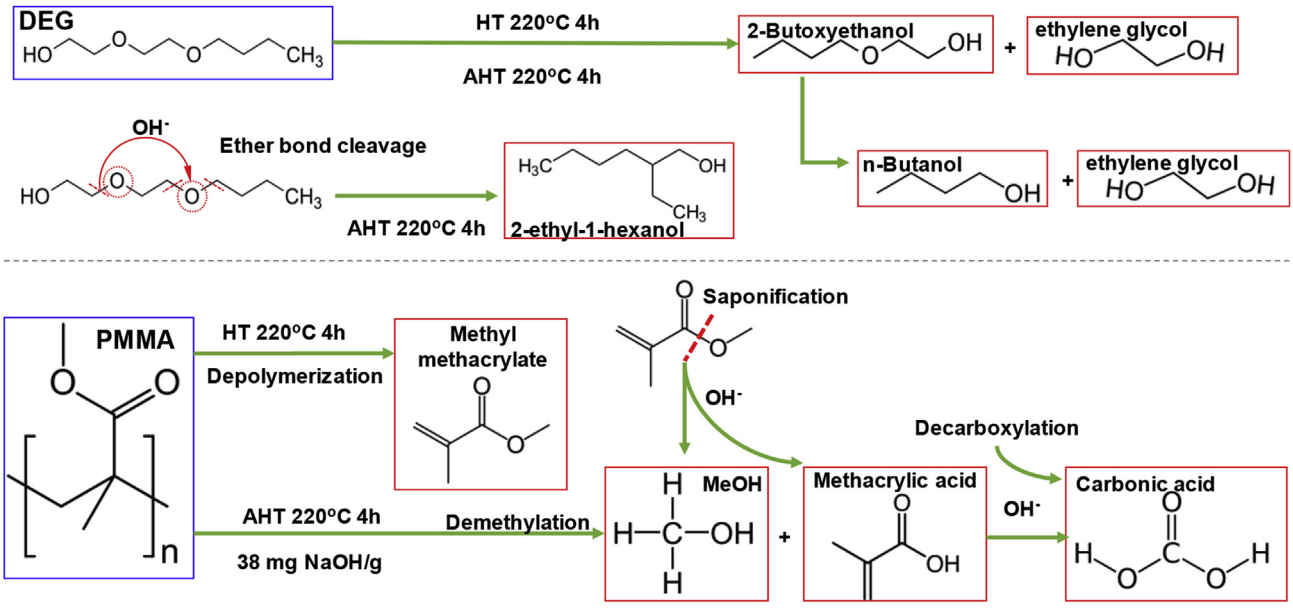

Fig. 6. Cleavage of ethers DEG to alcohols and PMMA degradation pathway during HT or AHT process.

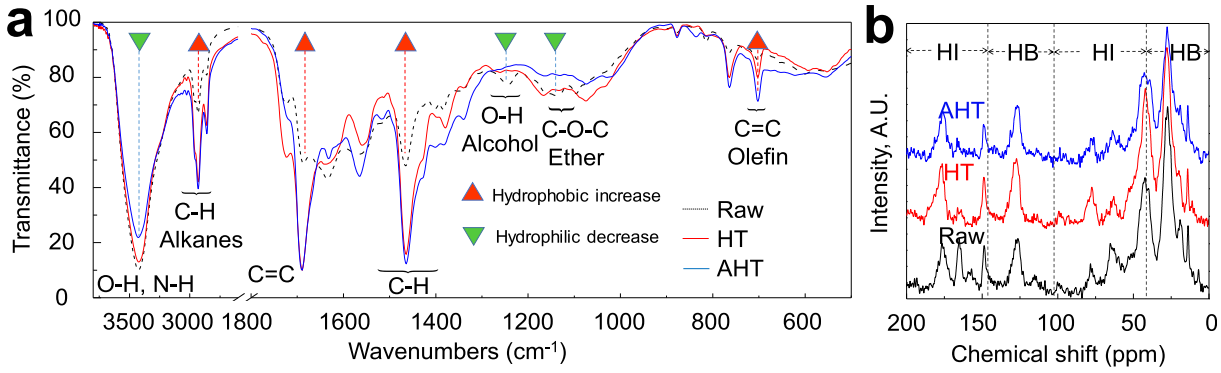

Fig. 7. Changes in functional groups as a result of treatment. (a) FTIR of solid samples from Raw WPS (dotted), after HT (red) or AHT processing (blue); (b) Solid-state 13C NMR of solid samples from Raw WPS (dotted), after HT (red) or AHT processing (blue). The two categories were labeled as HI (hydrophilic functional groups) or HB (hydrophobic functional groups). (For interpretation of the references to colour in this figure legend, the reader is referred to the Web version of this article.)

sludge (68.2 ± 1.5% and 50.1 ± 1.2%), high boiling residues from distillation tower (TMR 75.2% ± 3.6%) and concentrated solutions of fluorine industry (TMR 85.8 ± 4.7%). Furthermore, no significant weight change of five metal coupons (Stainless steel, Titanium, Nickel alloys, Zirconium alloy, and Hastelloy) was observed after five cycles of HT or AHT process (weight change < ±0.01%, Table S15), indicating that reactors made by either of these materials should resist corrosion by the hydrothermal chemical reactions. Thus, we scaled up this process using a 50 L pilot-scale batch hydrothermal system to treat WPS (Fig. S4b). Using an operating temperature of 220 °C with a reaction time of 4 h, we achieved TMR of 55.6 ± 6.7% (HT) and 69.8 ± 3.9% (AHT), DMR of 31.6 ± 5.4% (HT) and 40.9 ± 3.2% (AHT) (Table S16).

Table 2
Distribution of different carbon compounds in raw WPS and solids collected after HT and AHT treatment, calculated from ^{13}C NMR spectra[a].

Sample	Chemical shift δ (ppm)	Raw	HT	AHT
Carboxylic	220–161	6.87	8.16	7.05
Aromatic	161–113	10.39	11.65	12.75
Anomeric	113–93	3.22	1.91	2.65
Carbohydrate	93–44	15.84	15.44	12.11
Alkyl	44–0	63.68	62.84	65.44
HI/HB[b]		0.35	0.34	0.28

[a] The percentage of individual peak was calculated by dividing its area by the total spectral peak area.
[b] HI/HB is an empirical index of hydrophilicity, calculated based on the spectral areas as: ∑(Carboxylic + Anomeric + Carbohydrate) ÷ ∑(Aromatic + Alkyl); i.e., (δ(113–44) + δ(200–161))/(δ(44–0) + δ(161–113))[31].

4. Conclusions

This study addressed significant limitations associated with dewatering of hazardous organic wastes to achieve volume and dry mass reduction. We demonstrate that AHT can significantly reduce the volume and mass of various hazardous organic wastes, converting them to nonflammable, hydrophobic solid residues and biodegradable wastewater. The released water (with a higher ionic product) acts as a solvent under hydrothermal conditions to enhance the solubilization of organic matter to aqueous phase. This conversion contributes to dry mass reduction. Accompanied by demethylation of carbon chains, alkali triggers solid-solid interactions that increase exposure of hydrophobic functional groups

to the particle surface, forming hydrophobic matter to improve dewatering. This study provides the first evidence of a novel, reliable and scalable approach for hazardous organic wastes reduction with beneficial implications for environmental protection.

Notes

The authors declare no competing financial interest.

Declaration of interests

The authors declare that they have no known competing financial interests or personal relationships that could have appeared to influence the work reported in this paper.

Acknowledgements

This work was supported by Natural Science Foundation (NSF) of China (51878137, 51878136, 51878135); the Fundamental Research Funds for the Central Universities and the Donghua University Distinguished Young Professor Program; Shanghai Chen-Guang Program (17CG34); China Scholarship Council. We also appreciate the kind supports from SAIC-GM-Wuling Automobile (Liuzhou, China), Huf Automotive Lock Corp Ltd (Shanghai, China), Mars Foods Jiaxing Co Ltd (Jiaxing, China).

Appendix A. Supplementary data

Supplementary data to this article can be found online at https://doi.org/10.1016/j.watres.2019.02.050.

References

Aguado, J., Serrano, D.P., Escola, J.M., 2008. Fuels from waste plastics by thermal and catalytic processes: a review. Ind. Eng. Chem. Res. 47 (21), 7982–7992.
Akafuah, N.K., Toda, K., Salazar, A., Saito, K., 2013. Automotive Paint Spray Characterization and Visualization, Automotive Painting Technology. Springer, Dordrecht, The Netherlands, pp. 121–165.
Akiya, N., Savage, P.E., 2002. Roles of water for chemical reactions in high-temperature water. Chem. Rev. 102 (8), 2725–2750.
Allcock, H.R., 2008. Introduction to Materials Chemistry. John Wiley, New York, NY, USA.
Bennamoun, L., Arlabosse, P., Leonard, A., 2013. Review on fundamental aspect of application of drying process to wastewater sludge. Renew. Sustain. Energy Rev. 28, 29–43.
Cai, Q., Luo, Z.S., Pang, W.Q., Fan, Y.W., Chen, X.H., Cui, F.Z., 2001. Dilute solution routes to various controllable morphologies of MCM-41 silica with a basic medium. Chem. Mater. 13 (2), 258–263.
Chen, D.T., Perman, C.A., Riechert, M.E., Hoven, J., 1995. Depolymerization of tire and natural-rubber using supercritical fluids. J. Hazard Mater. 44 (1), 53–60.
Christensen, M.L., Keiding, K., Nielsen, P.H., Jorgensen, M.K., 2015. Dewatering in biological wastewater treatment: a review. Water Res. 82, 14–24.
Comisar, C.M., Hunter, S.E., Walton, A., Savage, P.E., 2008. Effect of pH on ether, ester, and carbonate hydrolysis in high-temperature water. Ind. Eng. Chem. Res. 47 (3), 577–584.
D'Alisa, G., Armiero, M., De Rosa, S.P., 2014. Rethink Campania's toxic-waste scandal. Nature 509 (7501), 427-427.
Daniels, S.L., 1986. Hazardous-waste disposal. Science 234 (4775), 412-412.
Demirbas, A., 2010. Sub- and super-critical water depolymerization of biomass. Energy Sources Part A 32 (12), 1100–1110.
Dmitrienko, M.A., Strizhak, P.A., 2018. Coal-water slurries containing petrochemicals to solve problems of air pollution by coal thermal power stations and boiler plants: an introductory review. Sci. Total Environ. 613, 1117–1129.
Fan, J.J., De Bruyn, M., Budarin, V.L., Gronnow, M.J., Shuttleworth, P.S., Breeden, S., Macquarrie, D.J., Clark, J.H., 2013. Direct microwave-assisted hydrothermal depolymerization of cellulose. J. Am. Chem. Soc. 135 (32), 11728–11731.
Garcia-Labiano, F., Gayan, P., Adanez, J., De Diego, L.F., Forero, C.R., 2007. Solid waste management of a chemical-looping combustion plant using Cu-based oxygen carriers. Environ. Sci. Technol. 41 (16), 5882–5887.
Guo, S.D., Liang, H., Bai, L.M., Qu, F.S., Ding, A., Ji, B., Wang, X., Li, G.B., 2019. Synergistic effects of wheat straw powder and persulfate/Fe(II) on enhancing sludge dewaterability. Chemosphere 215, 333–341.
Higgins, M.J., Beightol, S., Mandahar, U., Suzuki, R., Xiao, S., Lu, H.W., Le, T., Mah, J., Pathak, B., DeClippeleir, H., Novak, J.T., Al-Omari, A., Murthy, S.N., 2017. Pretreatment of a primary and secondary sludge blend at different thermal hydrolysis temperatures: impacts on anaerobic digestion, dewatering and filtrate characteristics. Water Res. 122, 557–569.
Jia, X.Q., Qin, C., Friedberger, T., Guan, Z.B., Huang, Z., 2016. Efficient and selective degradation of polyethylenes into liquid fuels and waxes under mild conditions. Sci. Adv. 2 (6), 1–7.
Jiang, H., Hu, J.Q., Gu, F., Li, C.Z., 2009. Stable field emission performance from urchin-like ZnO nanostructures. Nanotechnology 20 (5), 1–5.
Lee, D.J., Lee, S.F., 1995. Measurement of bound water-content in sludge - the use of differential scanning calorimetry (DSC). J. Chem. Technol. Biotechnol. 62 (4), 359–365.
Li, C.X., Wang, X.D., Zhang, A.G., Yu, G.W., Lin, J.J., Wang, Y., 2017. Hydrothermal and alkaline hydrothermal pretreatments plus anaerobic digestion of sewage sludge for dewatering and biogas production: bench-scale research and pilot-scale verification. Water Res. 117, 49–57.
Liaw, H.J., Gerbaud, V., Chen, C.C., Shu, C.M., 2010. Effect of stirring on the safety of flammable liquid mixtures. J. Hazard Mater. 177 (1–3), 1093–1101.
Lim, S.R., Kang, D., Ogunseitan, O.A., Schoenung, J.M., 2011. Potential environmental impacts of light-emitting diodes (LEDs): metallic resources, toxicity, and hazardous waste classification. Environ. Sci. Technol. 45 (1), 320–327.
Liu, K., Chen, Y.G., Xiao, N.D., Zheng, X., Li, M., 2015. Effect of humic acids with different characteristics on fermentative short-chain fatty acids production from waste activated sludge. Environ. Sci. Technol. 49 (8), 4929–4936.
Mursito, A.T., Hirajima, T., Sasaki, K., 2011. Alkaline hydrothermal de-ashing and desulfurization of low quality coal and its application to hydrogen-rich gas generation. Energy Convers. Manag. 52 (1), 762–769.
Roberts, V., Fendt, S., Lemonidou, A.A., Li, X.B., Lercher, J.A., 2010. Influence of alkali carbonates on benzyl phenyl ether cleavage pathways in superheated water. Appl. Catal. B Environ. 95 (1–2), 71–77.
Sadovnikov, S.I., Gusev, A.I., 2017. Synthesis and characterization of novel stellate sea-urchin-like silver particles with extremely low density and superhydrophobicity. J. Mater. Chem. 5 (38), 20289–20297.
Sahraneshin, A., Asahina, S., Togashi, T., Singh, V., Takami, S., Hojo, D., Arita, T., Minami, K., Adschiri, T., 2012. Surfactant-assisted hydrothermal synthesis of water-dispersible hafnium oxide nanoparticles in highly alkaline media. Cryst. Growth Des. 12 (11), 5219–5226.
Salihoglu, G., Salihoglu, N.K., 2016. A review on paint sludge from automotive industries: generation, characteristics and management. J. Environ. Manag. 169, 223–235.
Serrano, D.P., Aguado, J., Escola, J.M., 2012. Developing advanced catalysts for the conversion of polyolefinic waste plastics into fuels and chemicals. ACS Catal. 2 (9), 1924–1941.
Staszak, C.N., Malinowski, K.C., 1987. The pilot-scale demonstration of the modar oxidation process for the destruction of hazardous organic waste materials. Environ. Prog. 6 (1), 39–43.
Thomas, K.E., McCormick, L.J., Vazquez-Lima, H., Ghosh, A., 2017. Stabilization and structure of the cis tautomer of a free-base porphyrin. Angew. Chem. Int. Ed. 56 (34), 10088–10092.
Unterlass, M.M., 2018. Hot water generates crystalline organic materials. Angew. Chem. Int. Ed. 57 (9), 2292–2294.
Valsaraj, K.T., 1994. Hydrophobic compounds in the environment - adsorption equilibrium at the air-water-interface. Water Res. 28 (4), 819–830.
Walser, T., Limbach, L.K., Brogioli, R., Erismann, E., Flamigni, L., Hattendorf, B., Juchli, M., Krumeich, F., Ludwig, C., Prikopsky, K., Rossier, M., Saner, D., Sigg, A., Hellweg, S., Gunther, D., Stark, W.J., 2012. Persistence of engineered nanoparticles in a municipal solid-waste incineration plant. Nat. Nanotechnol. 7 (8), 520–524.
Wang, H., Hu, Y.H., 2013. Electrolyte-induced precipitation of graphene oxide in its aqueous solution. J. Colloid Interface Sci. 391, 21–27.
Wang, L.P., Li, A.M., 2015. Hydrothermal treatment coupled with mechanical expression at increased temperature for excess sludge dewatering: the dewatering performance and the characteristics of products. Water Res. 68, 291–303.
Xiao, K.K., Pei, K.Y., Wang, H., Yu, W.B., Liang, S., Hu, J.P., Hou, H.J., Liu, B.C., Yang, J.K., 2018. Citric acid assisted Fenton-like process for enhanced dewaterability of waste activated sludge with in-situ generation of hydrogen peroxide. Water Res. 140, 232–242.
Xu, Y., Xue, X.S., Dong, L., Nai, C.X., Liu, Y.Q., Huang, Q.F., 2018. Long-term dynamics of leachate production, leakage from hazardous waste landfill sites and the impact on groundwater quality and human health. Waste Manag. 82, 156–166.
Yin, F.B., Wang, D.L., Li, Z.F., Ohlsen, T., Hartwig, P., Czekalla, S., 2015. Study on anaerobic digestion treatment of hazardous colistin sulphate contained pharmaceutical sludge. Bioresour. Technol. 177, 188–193.
Yu, J., Guo, M.H., Xu, X.H., Guan, B.H., 2014. The role of temperature and CaCl2 in activated sludge dewatering under hydrothermal treatment. Water Res. 50, 10–17.
Zhang, K., Zhu, J.H., Zhou, Y., Wu, B.C., 2014. Analysis the fry-drying process of oily sludge sample. Chem. Eng. Res. Des. 92 (11), 2396–2403.
Zhang, N., Xiong, Y.F., Zhao, J.B., 2007. Conversion of a Direct Process high-boiling residue to monosilanes by a two-step catalysis approach. Res. Chem. Intermed. 33 (7), 613–622.
Zhu, J.J., Yang, Y., Chen, Y., Yang, L., Wang, Y.F., Zhu, Y.Z., Chen, H.J., 2018. Co-pyrolysis of textile dyeing sludge and four typical lignocellulosic biomasses: thermal conversion characteristics, synergetic effects and reaction kinetics. Int. J. Hydrog. Energy 43 (49), 22135–22147.